frontiers | Frontiers in Physics

TYPE Original Research
PUBLISHED 20 February 2024
DOI 10.3389/fphy.2024.1372204

OPEN ACCESS

EDITED BY
Wenxiang Xu,
Hohai University, China

REVIEWED BY
Lin Li,
China University of Petroleum, China
Raj Kumar Manna,
Northeastern University, United States
Bin Yan,
Sichuan University, China
Ling Zhang,
Zhengzhou University, China

*CORRESPONDENCE
Yuncheng Wang,
wangyc950902@foxmail.com

RECEIVED 17 January 2024
ACCEPTED 06 February 2024
PUBLISHED 20 February 2024

CITATION
Lu L, Wang F, Wang Y, Zhang J, Xiang L, Liu Z and Jiang J (2024), Probing the nanomechanics of interfacial interactions between hydrophobic surfaces.
Front. Phys. 12:1372204.
doi: 10.3389/fphy.2024.1372204

Probing the nanomechanics of interfacial interactions between hydrophobic surfaces

Liqun Lu[1,2], Fengjuan Wang[1], Yuncheng Wang[1]*, Jiawen Zhang[1], Li Xiang[3], Zhiyong Liu[1] and Jinyang Jiang[1]

[1]School of Materials Science and Engineering, Southeast University, Nanjing, China, [2]State Key Laboratory of High Performance Civil Engineering Materials, Jiangsu Research Institute of Building Science Co. Ltd., Nanjing, China, [3]School of Mechanical Engineering, Southeast University, Nanjing, China

Hydrophobic interactions are widely applied in diverse fields, yet the effect of the degree of hydrophobicity on the interactions between hydrophobic surfaces is still unaddressed, limiting the development of functional hydrophobic surfaces. In this study, the interfacial interactions and configuration of hydrophobic chains on surfaces with ranging hydrophobicity are surveyed by surface forces apparatus. Our findings revealed that with partial hydrophobicity, a long-range electrical double-layer repulsive force pertains between surfaces, while between fully hydrophobized surfaces, only steric hindrance is observed, and the hydrophobic chains maintain configuration even after long time compression. Our findings provide useful implications for understanding hydrophobic interactions.

KEYWORDS

hydrophobic interaction, surface hydrophobilization, surface forces, alkyl chain, nanomechanics

Introduction

Hydrophobic interactions widely exist in biological systems, such as in the formation of bilayer membrane lipids [1] and the folding of proteins, [2], as well as in engineering processes [3–5], including the bubble attachment in mineral flotation [6], bubble directional transport [7], and oil–water separation [3, 8–10]. Therefore, it is of vital significance to understand the interfacial interaction mechanism between hydrophobic surfaces in aqueous media, which could provide useful implications in understanding natural and engineering behavior and in guiding the development of hydrophobic surfaces with designed wettability.

The range and strength of hydrophobic interactions are in the scale of nanometer and tens of nanonewton, respectively; hence, its measurement requires a high resolution of both force and distance. Previously, the hydrophobic interactions between bubbles have been successfully measured by atomic force microscopy (AFM) coupled with reflection interference contrast microscopy [11]. The force measurement with high precision was achieved by AFM, while the distance measurement with a subnanometer resolution was enabled by the light interference between bubble–liquid and liquid–bubble interfaces. However, such techniques cannot be extended to the solid–solid interface measurement because most solid substrates and cantilevers are opaque. Surface forces apparatus (SFA) is employed to use cleaved mica as a solid substrate, of which the back is coated by a thin silver film [12, 13]. As such, the light reference is enabled between the silver–mica and mica–silver

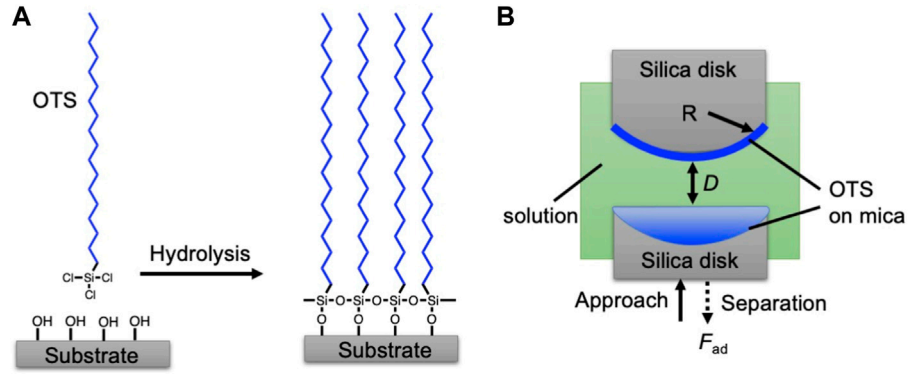

FIGURE 1
(A) Illustrative grafting procedure of OTS on the mica surface. **(B)** Schematic setup of surface forces apparatus (SFA). The targeted OTS coated mica was glued on the silica disk. The aqueous solution was injected into the chamber. During the force measurement, the opposed OTS-coated surfaces were brought together until contact and then separated to measure the adhesion force (F_{ad}).

interfaces, and then, the distance between mica surfaces can be precisely measured [14]. A high-precision force measurement, i.e., 10^{-8} N, can also be realized by SFA via spring deflection. By using such a technique, the force measurement between hydrophobic surfaces was performed [15]. The mica surface was hydrophobized by vacuum deposition of octadecyltrichlorosilane (OTS), which is one of the most common reactive silanes in surface hydrophobilization. In a previous study, the interactions between two hydrophobic surfaces during approaching were analyzed, and it was found that only the force curves between relatively short deposition times could be described by the Derjaguin–Landau–Verwey–Overbeek (DLVO) theory [16]. For surfaces with longer deposition times, the significant role of hydrophobic surfaces and steric interactions deviates the force–distance curve from the DLVO model. Such findings provide important insights in understanding the approaching process between hydrophobic solid surfaces. However, the distance range of the electrical double-layer and steric hindrance and the configuration rearrangement of the hydrophobic chains under external force are still unclear, which is also vital for affecting the repulsion, attachment, and separation of hydrophobic surfaces.

In this study, the detailed interactions between surfaces with wettability ranging between hydrophilic, partially hydrophobic, and hydrophobic surfaces are investigated by the SFA technique. OTS was chosen as the hydrophobizing agent due to the wide application of alkane in solid surface hydrophobilization [17], emulsion stabilization [18, 19], and its existence in membrane lipids [20]. By using the solution deposition method in ethanol, the deposition density of OTS on mica was modulated by controlling the deposition time. The distance range of electrical double-layer and steric hindrance was carefully analyzed, the adhesion force and film thickness after compression were measured, and then, the configuration of the alkyl chain of OTS on mica surfaces was proposed. Our findings unravel detailed information on the interaction between alkyl chain-grafted surfaces with varied wettability, which can provide fundamental insights into various engineering and biological processes with hydrophobic interactions involved.

Materials and methods

Materials

Octadecyltrichlorosilane (OTS, 95%), absolute ethanol, and sodium chloride (anhydrous, 99.999%) were purchased from Shanghai Aladdin Bio-Chem Technology Co., Ltd. Deionized (DI) water was used for all sample preparation and rinsing. An atomically smooth mica sheet was cleaved from muscovite ruby mica and used freshly [21, 22].

OTS deposition on the mica surface

The cleaved mica surfaces for determining the AFM measurement were treated by plasma for 10 min for hydroxylation. Then, the treated mica sheets were soaked in the ethanol solution with 3 vol% of OTS (Figure 1A) for 4, 8, and 12 h, respectively. Subsequently, the surface was washed with ethanol and dried by nitrogen flush.

The preparation of the mica surface used for determining SFA measurements was carried out herein. Mica sheets of a thickness of 1–5 μm were freshly cleaved and attached on a thick mica substrate, and then, a silver layer with a thickness of ~45–55 nm was coated on their back side by magnetron sputtering. Subsequently, the back-silvered mica sheet was attached to a silica disk with a radius R of ~2 cm. Then, the mica surface was coated by OTS by following the procedure described above.

Characterizations

The grafting density of OTS on mica surfaces was surveyed by Fourier-transform infrared (FTIR) spectrometry (Thermo Scientific, Nicolet iS10). Bare mica was chosen as the background reference. The surface morphology was characterized by the AFM technique (Bruker, Dimension ICON). The force measurement was performed using the SFA 2000 system (SurForce, LLC). In the force measurement, two bare mica surfaces in a dry state were first brought together and then separated vertically using an electric motor. The zero-separation distance was then determined by the visualization of the light interference fringes of the opposed mica surfaces by multiple-beam interferometry by using the interference

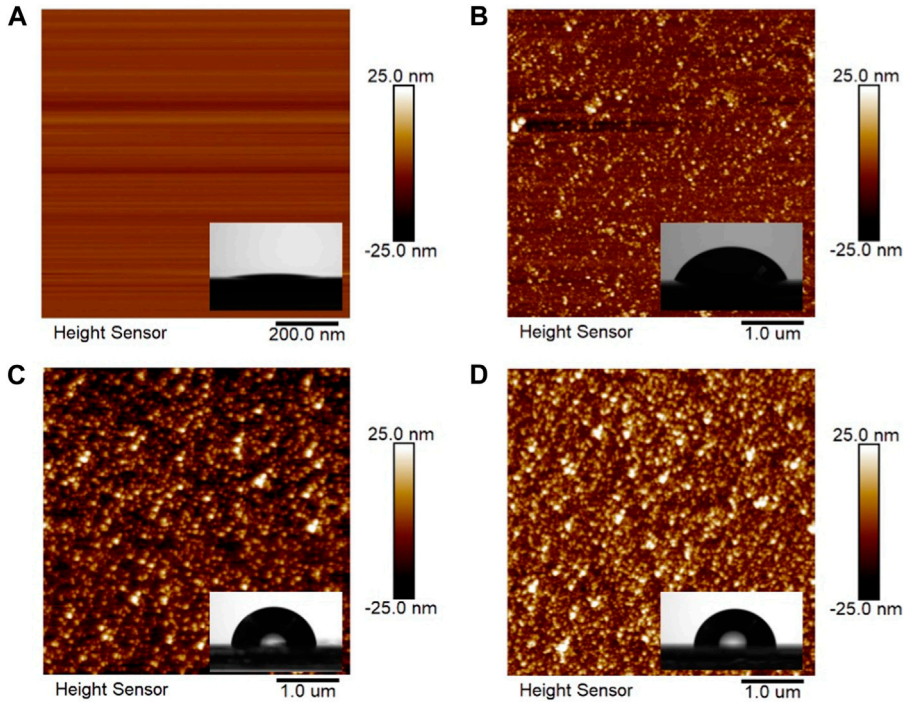

FIGURE 2
Atomic force microscopy (AFM) images of **(A)** bare mica and OTS-coated mica surfaces with a deposition time of **(B)** 4 h, **(C)** 8 h, and **(D)** 12 h.

fringes of equal chromatic order (FECO) [16, 23, 24]. Then, the force measurement between the OTS-coated surfaces was determined by pre-filling the SFA chamber with 1 mM of the NaCl solution (Figure 1B). The opposed coated surfaces were driven toward each other, brought into contact for 30 min, and then separated. Then, the force–distance profile between the surfaces was recorded. Surface interactions between bare mica in 1 mM of NaCl solution were also measured for comparison. The water contact angle measurement was performed using a contact angle goniometer (LAUDA Scientific) with the model number OSA 100. The water droplet size was ~15 μm.

Results and discussion

The illustrative preparation procedure of OTS coating on the mica surface is shown in Figure 1A. In the anhydrous ethanol solution, the Si-Cl group of OTS undergoes hydrolysis in the presence of trace moisture in the air and then grafts on the hydroxyl group on mica [25]. To increase the hydroxyl group density, the mica surfaces were treated with plasma before the OTS coating [26]. The grafting density of OTS was controlled by the soaking time (4h, 8h, and 12 h).

The coverage of OTS on the mica surface is characterized by AFM. As shown in Figure 2A, the bare mica surface is atomically smooth, and the surface shows superhydrophilicity with a water contact angle of less than 5°. After 4 h of deposition, the nanoaggregate appears on the mica surface (Figure 2B), suggesting the successful deposition of OTS on the mica surface. The water contact angle of ~63.0° confirms the existence of OTS and demonstrates that the surface, namely, OTS-4h, is partially hydrophobic. After 8 h of deposition, the AFM image shows almost full coverage (Figure 2C), and the contact angle reaches ~92.0° [27]. With 12 h of deposition, the grafting density of OTS on mica further increases and shows a negligible ungrafted area (Figure 2D), with the contact angle gradually increasing to ~97.9°.

To further validate the deduction on the surface grafting density of OTS on mica surfaces, the Fourier-transform infrared (FTIR) spectra of the specimen were acquired. The bare mica surface was chosen as the background reference, which was deducted during the FTIR measurement of specimens. The peaks at the wavenumber ranging from ~500 to ~1,100 cm^{-1} should be ascribed to the mica substrate [28], which were normalized to observe the transmittance intensity of the peaks attributed to OTS. As shown in Figure 3B, the characteristic peaks at 2,849.8 and 2,917.8 cm^{-1} belong to OTS [29], suggesting its successful grafting on all the specimens. However, the intensity of the peaks at these regions of OTS-4h is evidently lower, while the intensities of those of OTS-8h and OTS-12 h are quite similar to each other, suggesting the almost graft saturation of OTS after 8 h of coating. As such, comprehensively combining the results of AFM imaging, the water contact angle measurement, and FTIR spectra, the deposition behavior of the OTS on mica with increasing deposition time was proposed, as shown in Figure 3C. At a deposition time of ~4 h, the grafting of OTS on the mica substrate is sparse, with plenty of space for the subsequent deposition, which was consistent with the AFM image (Figure 2B) showing sparse aggregates were observed on the mica surface. Because ethanol is a benign solvent for OTS, the illustrative configuration of the alkyl chain in OTS is unfolded. When the deposition increases to ~8 h, the grafting density of OTS dramatically increases, and there is barely any space for further grafting on the mica surface, which is supported by the much higher

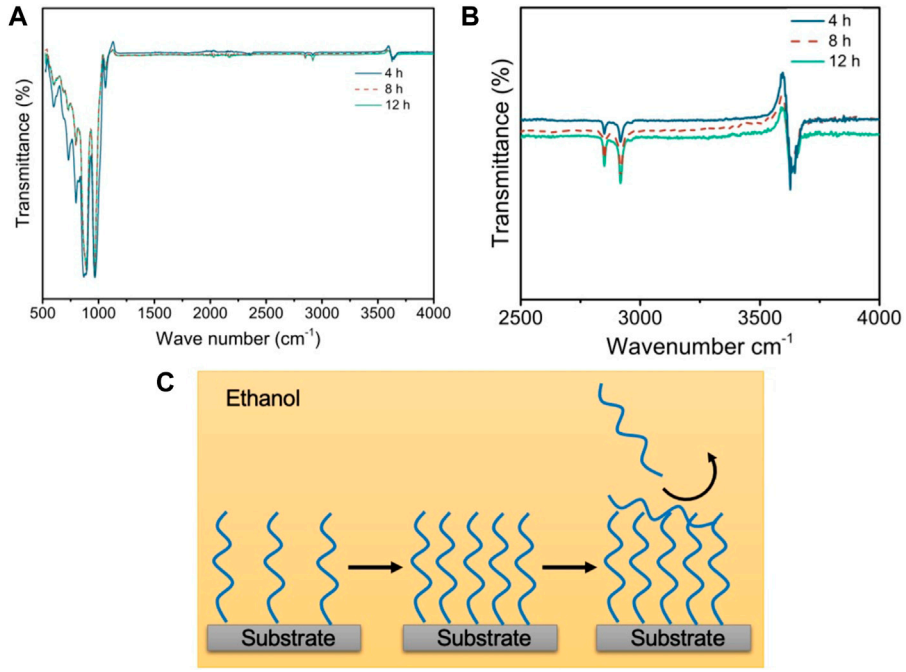

FIGURE 3
(A) Fourier-transform infrared (FTIR) spectra of OTS-coated mica surfaces with a deposition time of 4, 8, and 12 h. **(B)** Selectively enlarged region in panel a showing the spectra with the wavenumber ranging from 2,500 to 4,000 cm^{-1}. **(C)** Illustrative deposition process of OTS on the mica surface in the ethanol solution.

and almost full coverage of aggregates on the mica shown in Figure 2C. As such, by increasing the deposition time to ~12 h, the coverage of OTS on the mica surface increases only slightly and the superfluous OTS on the surface can only weakly associate on the mica surface via hydrophobic interactions between the alkyl chains, most of which should be washed away after rinsing with ethanol. Therefore, it can be proposed that OTS-4h is partially hydrophobic, OTS-8h is almost fully hydrophobic, and OTS-12 h is fully hydrophobic.

The interfacial interactions between the surfaces with different hydrophobicity levels are then carefully surveyed by the SFA technique. The two opposed surfaces are first driven toward each other. When the surfaces are close, a repulsive force is detected. At this point, the distance is denoted as $2D_A$, which is double the thickness of the absorbed film or the grafted coating on the surface. Upon further approaching, such films could be evicted or compressed. When the distance between the opposed surfaces does not change with increasing compressive force, the thickness of the "hardwall," $2D_T$, is measured. Such thickness should correspond to the rigid, strongly absorbed/chemically grafted layer. The surfaces are further kept in contact for 30 min and then driven apart from each other. During the separation, the adhesive force is measured and then normalized as $|F_{ad}/R|$. The specific salt concentration utilized in this study was selected as 1 mM NaCl, the concentration of which could fix the Debye length to ~10 nm to stabilize the electric double-layer (EDL) repulsion in an aqueous system for hydrophobic force measurement [30, 31]. The reason is explained as follows: 1) in a background solution with a low NaCl concentration, the amount of ions dissociated from the surface and dissolved in the water, although low, is uncontrollable and will significantly impact the Debye length, resulting in the Debye length to be uncertain for the tested system [16]; 2) in a background solution with a high NaCl concentration, although the Debye length can be determined, the high NaCl concentration can dramatically weaken the hydrophobic interaction, thus negatively affecting the investigation on the impact of surface hydrophobicity on the hydrophobic interaction-induced nanomechanics [32].

For bare mica, the repulsive force was detected during the approach and D_A is measured as ~10 nm. The repulsion at this range should be ascribed to the weakly absorbed electrical double-layer and hydration repulsion at the surface based on previous studies (Figure 4A) [30, 33]. Upon the compression, the weakly absorbed electric double-layer is evicted, and only the strongly absorbed hydrated counterions stay on the surface, of which the thickness, D_T, is measured as ~2.3 nm. During the separation, because of the absorbed hydration layer on both mica surfaces, a negligible adhesive force is detected. Such an observation is consistent with previous studies [33]. For OTS-4h, as shown in Figure 4B, D_A is also measured as ~10 nm, and D_T is measured as ~2.5 nm. Based on the topological AFM image in combination with the FTIR spectra, a low density of OTS was grafted on the mica surface, leading to a relatively increased WCA to ~63°. The low OTS graft density suggests a large average distance between grafted sites of OTS chains; in light of this, the large space around each chain allows the chains to adopt a mushroom-like configuration to collapse on the surface, as illustrated in the **inset of** Figure 4B. Therefore, in this situation, the collapsed OTS chain grafted on the mica surface could only slightly increase the

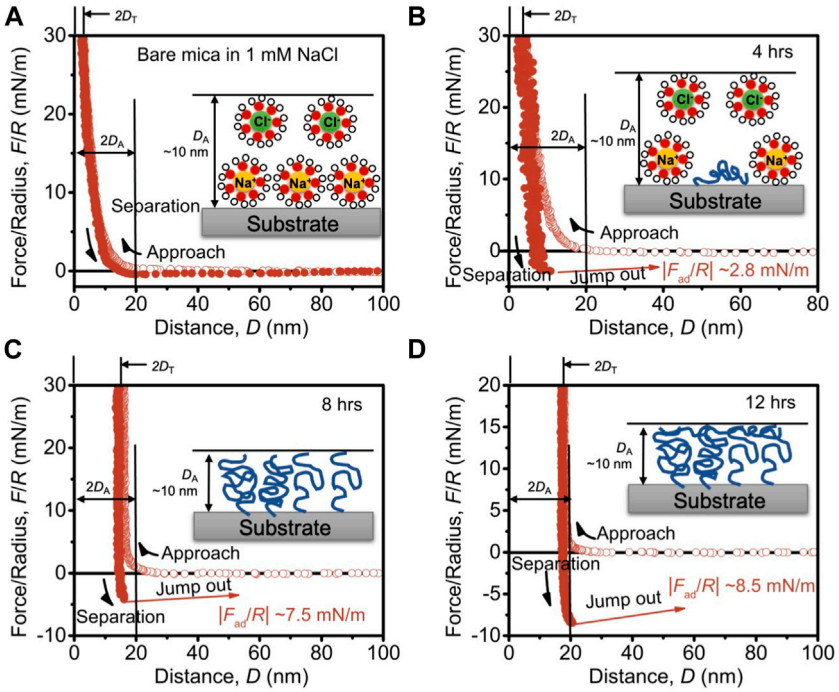

FIGURE 4
SFA force–distance curves between surfaces of **(A)** bare mica, **(B)** OTS-4h, **(C)** OTS-8h, and **(D)** OTS-12 h. The solid circle lines indicate the approaching force–distance curve, and the open circle lines represent the curve during separation. D_A is the thickness of the absorbed or grafted film on the mica surface observed during the approach. D_T is denoted as the thickness of the hardwall, which is the thickness of the film on the mica surface upon compression. $|F_{ad}/R|$ is the normalized adhesion force between surfaces. The insets show the absorption of hydrated ions and the configuration of OTS chains on the mica surface with the range of D_A denoted.

hardwall thickness D_T, and then, the measured D_A should be still attributed to the weakly absorbed electrical double-layer, which is squeezed away during approaching and leaves the lean OTS on the mica surface to be measured as D_T. During the separation, weak adhesion is measured as ~2.8 mN/m. This adhesive force should originate from the attractive hydrophobic force between the opposed OTS-modified surfaces, and the relatively low value should be due to the low surface coverage of OTS. As to OTS-8h, D_A is similarly measured as ~10 nm, yet D_T shows a distinct difference compared with the previous specimens, which significantly increases to ~7.2 nm. Combining with the AFM images that show closely packed moieties and a significantly increased WCA of ~92.0°, in this case, the surface should be almost fully covered by OTS, and thus, the measured D_A, although coinciding with the previous specimens, should be ascribed to the steric hindrance of the OTS chains. In addition, the slightly decreased thickness under compression, i.e., D_T, should be due to the segment rearrangement of the alkyl chain under eternal force. Moreover, because of such a chain rearrangement, the opposed OTS surfaces could contact each other better. Therefore, due to the dramatically higher OTS coverage, although relatively high roughness is observed in the AFM image (Figure 2C), strong adhesion is still measured (~7.5 mN/m). With further increasing the deposition time to 12 h, the value of D_A is still close to the previous measurement (Figure 4D), suggesting that the thickness of the OTS grafting is similar to OTS-8h, which is in accordance with the previous assumption. Contrastingly, D_T evidently increases to ~8.6 nm.

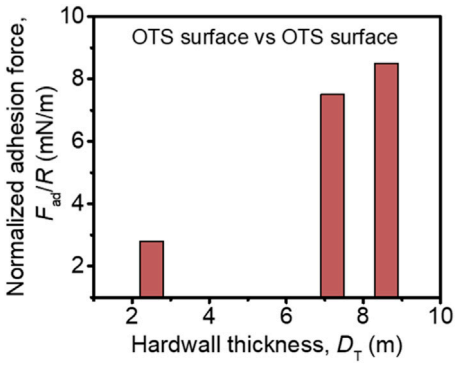

FIGURE 5
Normalized adhesion force as a function of the hardwall thickness of OTS.

Such an observation indicates that the OTS film on OTS-12 h is more rigid than OTS-8h, which can be ascribed to the absorption of the OTS chain on the top of the grafted OTS molecules. Slightly increased WCA and enhanced FTIR characteristic peaks corroborated more OTS chains deposited on the surface. Synergistically, due to the more compact OTS on the opposed surfaces, the adhesive force further increases to ~8.5 mN/m. From the discussion above, it can be suggested that the adhesion force is highly correlated with the OTS coverage, while D_T could be used to evaluate the coverage of OTS. Thus, the adhesion force as a

function of D_T is shown in Figure 5 to better demonstrate the dependence of the adhesion force on D_T.

As such, with the high-precision measurement of thickness and adhesive force, the interaction mechanism and configuration rearrangement of the alkyl chain on surfaces with varying wettability are comprehensively analyzed and unraveled, providing fundamental insights into the understanding of the interfacial interactions between hydrophobic surfaces.

Conclusion

The high-precision measurement of the interfacial interaction force and distance between surfaces with high hydrophilicity, partial hydrophobicity, and high hydrophobicity has been performed by the SFA technique. It is unraveled that 4 h of OTS coating only induces a low grafting density of OTS on mica. In this case, there is still strong electric double-layer repulsion upon approach, the thickness of OTS coating on the surface in water is quite low, and the OTS molecule should be lean on the mica surface. With 8 h of OTS deposition, the repulsion measured during the approach should mainly arise from steric hindrance. The OTS molecule should be densely grafted on the surface and show strong adhesive hydrophobic interactions. With 12 h of OTS deposition, although the hydrophobicity of the surface increases only slightly, the more compact OTS molecules induce evidently increased hydrophobic interaction. In biological systems, hydrophobic domains widely exist in biological molecules, e.g., the alkyl chain of the lipid molecule in the membrane and the nonpolar (hydrophobic) side chains in protein; thus, there are hydrophobic interactions between them. The hydrophobic interactions dominantly drive the assembly of the lipid membrane, the protein folding, and the anchor of functional protein on the lipid membrane. Understanding the fundamentals of hydrophobic interactions can provide insights into the assembly behavior of those biological molecules containing hydrophobic domains. Therefore, this study not only provides useful insights into the understanding of the biological behavior of tissues, such as the lipid membrane interaction and protein folding, but also in designing advanced functional materials with tunable hydrophobicity.

Data availability statement

The raw data supporting the conclusion of this article will be made available by the authors, without undue reservation.

Author contributions

LL: conceptualization, data curation, formal analysis, investigation, methodology, writing–original draft, and writing–review and editing. FW: methodology, project administration, resources, and writing–review and editing. YW: data curation, writing–review and editing, and methodology. JZ: funding acquisition, project administration, resources, and writing–review and editing. LX: funding acquisition, project administration, resources, and writing–review and editing. ZL: formal analysis, funding acquisition, project administration, resources, supervision, and writing–review and editing. JJ: formal analysis, funding acquisition, project administration, resources, supervision, and writing–review and editing.

Funding

The author(s) declare financial support was received for the research, authorship, and/or publication of this article. This study was supported by the National Key Research and Development Program of China (2021YFB2601200), the Funds for International Cooperation and Exchange of the National Natural Science Foundation of China (52261160646), the Science Foundation for Distinguished Young Scholars of Jiangsu Province (BK20220071), and the Fundamental Research Funds for the Central Universities (RF1028623199).

Conflict of interest

Author LL was employed by Jiangsu Research Institute of Building Science Co. Ltd.

The remaining authors declare that the research was conducted in the absence of any commercial or financial relationships that could be construed as a potential conflict of interest.

The author(s) declared that they were an editorial board member of Frontiers, at the time of submission. This had no impact on the peer review process and the final decision.

Publisher's note

References

1. Takechi-Haraya Y, Ohgita T, Kotani M, Kono H, Saito C, Tamagaki-Asahina H, et al. Effect of hydrophobic moment on membrane interaction and cell penetration of apolipoprotein E-derived arginine-rich amphipathic α-helical peptides. *Scientific Rep* (2022) 12(1):4959. doi:10.1038/s41598-022-08876-9

2. Baldwin RL, Rose GD. How the hydrophobic factor drives protein folding. *Proc Natl Acad Sci* (2016) 113(44):12462–6. doi:10.1073/pnas.1610541113

3. Lu X, Dong W, Gao Z, He C, Chen S, Yang Q, et al. Doping nanocellulose crystal with poly(vinyl alcohol) for water-resistant composite fibers with enhanced mechanical and dyeing performances. *Polym Eng Sci* (2023) 63(7):2121–8. doi:10.1002/pen.26350

4. An N, Zhu Y, Wang X, Li Y, Liu J, Fang X, et al. Dual nanofillers-reinforced noncovalently cross-linked polymeric composites with unprecedented mechanical strength. *CCS Chem* (2023) 5(10):2312–23. doi:10.31635/ccschem.022.202202496

5. Wang G, Xiang J, Lin J, Xiang L, Chen S, Yan B, et al. Sustainable advanced fenton-like catalysts based on mussel-inspired magnetic cellulose nanocomposites to effectively remove organic dyes and antibiotics. *ACS Appl Mater Inter* (2020) 12(46):51952–9. doi:10.1021/acsami.0c14820

6. Xie L, Shi C, Cui X, Zeng H. Surface forces and interaction mechanisms of emulsion drops and gas bubbles in complex fluids. *Langmuir* (2017) 33(16):3911–25. doi:10.1021/acs.langmuir.6b04669

7. Yang C, Kuang Y, Zheng J, Liu L, Chen G. Controllable and directional transportation of bubbles on asymmetric hexagonal cage substrate in aqueous environment. *J Phys Chem Lett* (2022) 13(39):8993–8. doi:10.1021/acs.jpclett.2c02440

8. Beattie JK, Djerdjev AM. The pristine oil/water interface: surfactant-free hydroxide-charged emulsions. *Angew Chem Int Edition* (2004) 43(27):3568–71. doi:10.1002/anie.200453916

9. Dong W, Li J, Zhou Y, Li X, Wang G, Chen S, et al. Superhydrophilic microfibrous adsorbent with broad-spectrum binding affinity to effectively remove diverse pollutants from aqueous solutions. *Sep Purif Tech* (2023) 309:123051. doi:10.1016/j.seppur.2022.123051

10. Li L, Chen J, Jin X, Wang Z, Wu Y, Dai C. Novel polyhydroxy anionic surfactants with excellent water-solid interfacial wettability control capability for enhanced oil recovery. *J Mol Liquids* (2021) 343:116973. doi:10.1016/j.molliq.2021.116973

11. Shi C, Cui X, Xie L, Liu Q, Chan DYC, Israelachvili JN, et al. Measuring forces and spatiotemporal evolution of thin water films between an air bubble and solid surfaces of different hydrophobicity. *ACS Nano* (2015) 9(1):95–104. doi:10.1021/nn506601j

12. Li L, Yan B, Yang J, Chen L, Zeng H. Novel mussel-inspired injectable self-healing hydrogel with anti-biofouling property. *Adv Mater* (2015) 27(7):1294–9. doi:10.1002/adma.201405166

13. Yan B, Huang J, Han L, Gong L, Li L, Israelachvili JN, et al. Duplicating dynamic strain-stiffening behavior and nanomechanics of biological tissues in a synthetic self-healing flexible network hydrogel. *ACS Nano* (2017) 11(11):11074–81. doi:10.1021/acsnano.7b05109

14. Zhang J, Zeng H. Intermolecular and surface interactions in engineering processes. *Engineering* (2021) 7(1):63–83. doi:10.1016/j.eng.2020.08.017

15. Huang J, Liu X, Qiu X, Xie L, Yan B, Wang X, et al. Octadecyltrichlorosilane deposition on mica surfaces: insights into the interface interaction mechanism. *The J Phys Chem B* (2017) 121(14):3151–61. doi:10.1021/acs.jpcb.7b00828

16. Israelachvili JN. *Intermolecular and surface forces*. 3rd ed. Academic Press (2011).

17. Song JE, Phenrat T, Marinakos S, Xiao Y, Liu J, Wiesner MR, et al. Hydrophobic interactions increase attachment of gum Arabic-and PVP-coated Ag nanoparticles to hydrophobic surfaces. *Environ Sci Technol* (2011) 45(14):5988–95. doi:10.1021/es200547c

18. Zanini M, Marschelke C, Anachkov SE, Marini E, Synytska A, Isa L. Universal emulsion stabilization from the arrested adsorption of rough particles at liquid-liquid interfaces. *Nat Commun* (2017) 8(1):15701. doi:10.1038/ncomms15701

19. Wang Z, Dai C, Liu J, Dong Y, Liu J, Sun N, et al. Anionic-nonionic and nonionic mixed surfactant systems for oil displacement: impact of ethoxylate chain lengths on the synergistic effect. *Colloids Surf A: Physicochemical Eng Aspects* (2023) 678:132436. doi:10.1016/j.colsurfa.2023.132436

20. Harayama T, Riezman H. Understanding the diversity of membrane lipid composition. *Nat Rev Mol Cel Biol* (2018) 19(5):281–96. doi:10.1038/nrm.2017.138

21. Kékicheff P, Marcelja S, Senden TJ, Shubin VE. Charge reversal seen in electrical double layer interaction of surfaces immersed in 2:1 calcium electrolyte. *J Chem Phys* (1993) 99(8):6098–113. doi:10.1063/1.465906

22. Tan Q, Zhao G, Qiu Y, Kan Y, Ni Z, Chen Y. Experimental observation of the ion–ion correlation effects on charge inversion and strong adhesion between mica surfaces in aqueous electrolyte solutions. *Langmuir* (2014) 30(36):10845–54. doi:10.1021/la5024357

23. Israelachvili J, Min Y, Akbulut M, Alig A, Carver G, Greene W, et al. Recent advances in the surface forces apparatus (SFA) technique. *Rep Prog Phys* (2010) 73(3):036601. doi:10.1088/0034-4885/73/3/036601

24. Israelachvili JN. Thin film studies using multiple-beam interferometry. *J Colloid Interf Sci* (1973) 44(2):259–72. doi:10.1016/0021-9797(73)90218-x

25. Chi H, Quan W, Zhang J, Zhao L, Fang J. Advances in anti-relaxation coatings of alkali-metal vapor cells. *Appl Surf Sci* (2020) 501:143897. doi:10.1016/j.apsusc.2019.143897

26. Lee JH, Park JW, Lee HB. Cell adhesion and growth on polymer surfaces with hydroxyl groups prepared by water vapour plasma treatment. *Biomaterials* (1991) 12(5):443–8. doi:10.1016/0142-9612(91)90140-6

27. Tuteja A, Choi W, Mabry JM, McKinley GH, Cohen RE. Robust omniphobic surfaces. *Proc Natl Acad Sci* (2008) 105(47):18200–5. doi:10.1073/pnas.0804872105

28. Sohrabpour K, Mohamadi S, Abdollahzadeh Sharghi E, Abdouss M. Performance evaluation of novel Mica@reduced graphene oxide fixed rotating disk reactor in treatment of anaerobically reduced textile dyeing wastewater containing aromatic amines. *J Chem Tech Biotechnol* (2021) 96(7):2072–85. doi:10.1002/jctb.6742

29. Wu C, Liu Q, Liu J, Chen R, Takahashi K, Liu L, et al. Hierarchical flower like double-layer superhydrophobic films fabricated on AZ31 for corrosion protection and self-cleaning. *New J Chem* (2017) 41(21):12767–76. doi:10.1039/c7nj02684f

30. Pashley RM. DLVO and hydration forces between mica surfaces in Li+, Na+, K+, and Cs+ electrolyte solutions: a correlation of double-layer and hydration forces with surface cation exchange properties. *J Colloid Interf Sci* (1981) 83(2):531–46. doi:10.1016/0021-9797(81)90348-9

31. Israelachvili JN, Adams GE. Measurement of forces between two mica surfaces in aqueous electrolyte solutions in the range 0–100 nm. *J Chem Soc Faraday Trans 1: Phys Chem Condensed Phases* (1978) 74:975–1001. doi:10.1039/f19787400975

32. Faghihnejad A, Zeng H. Hydrophobic interactions between polymer surfaces: using polystyrene as a model system. *Soft Matter* (2012) 8(9):2746–59. doi:10.1039/c2sm07150a

33. Maier GP, Rapp MV, Waite JH, Israelachvili JN, Butler A. Adaptive synergy between catechol and lysine promotes wet adhesion by surface salt displacement. *Science* (2015) 349(6248):628–32. doi:10.1126/science.aab0556